Hybrid Anion and Proton Exchange Membrane Fuel Cells

Murat Ünlü, Junfeng Zhou, and Paul A. Kohl*

School of Chemical and Biomolecular Engineering, Georgia Institute of Technology, Atlanta, Georgia 30332-0100

Received: April 8, 2009; Revised Manuscript Received: May 13, 2009

A novel hybrid fuel cell is described using at least one electrode operating at high pH in an effort to use the high conductivity of Nafion and exploit the electrochemical advantages of high-pH operation. The electrochemical behavior of a hybrid anion exchange membrane (AEM)/proton exchange membrane (PEM) junction and corresponding fuel cell are presented. Two AEM/PEM junctions and fuel cells have been evaluated: AEM anode/PEM cathode and PEM anode/AEM cathode. The AEM cathode/PEM membrane configuration causes proton−hydroxide recombination at the membrane junction, resulting in self-hydration of the membrane. The fuel cell performance improves at lower relative humidity. At 65 °C and 0% relative humidity, the hybrid cell operates at steady state whereas the performance of a conventional PEM cell decreases with time due to dry-out.

Introduction

Fuel cells have the potential to provide clean and efficient energy sources for stationary, traction, and portable applications.[1] Among the various types of fuel cells, the proton exchange membrane fuel cell (PEMFC) has several desirable features including a high level of development. Although PEMFCs have been successfully used in numerous applications, there are several obstacles that impede wide-scale commercialization. These issues include sluggish reaction kinetics, complex water management, carbon monoxide poisoning, limited lifetime due to membrane and electrode degradation, and the high cost of noble-metal catalysts and perfluorinated membranes.[2−4]

Recent developments and the need for lower cost and more efficient fuel cells have created interest in anion exchange membrane fuel cells (AEMFCs).[5] The use of metal-free AEMs avoids CO_2 poisoning (i.e., precipitation of carbonate salts), which is the major obstacle in conventional alkaline fuel cells using sodium or potassium hydroxide as the electrolyte.[6]

The high-pH environment within the AEM fuel cell addresses many of the shortfalls with PEM-based fuel cells. The major advantages of AEM-based fuel cells include the following: (i) the more facile electrokinetics allow for the use of non-noble metals, such as silver and nickel as catalysts;[7] (ii) the wide selection of catalytic metals potentially extends the opportunity for selective catalysis; (iii) the direction of ion migration is from the cathode to the fuel anode (opposite that of a PEM-based fuel cell), which may lower fuel crossover because electro-osmotic drag is in the opposite direction; (iv) the use of hydrocarbon membranes in place of a perfluorinated membrane may lower the cost of materials; (v) more facile CO oxidation in an alkaline environment may significantly reduce CO poisoning.[8]

Although AEMFCs offer important potential advantages, the lower ionic conductivity of AEMs compared to Nafion is a concern because it may lower the performance. Recent efforts have resulted in ionic conductivities of 20−30 mS/cm, which are lower than the conductivity of Nafion (ca. 92 mS/cm).[9]

* To whom correspondence should be addressed. E-mail: kohl@gatech.edu.

TABLE 1: Physical Properties of the AEM Membrane Used in This Study[a]

ionic functional group	$-N^+(CH_3)_3OH^-$
conductivity (mS/cm)	21.2
water uptake (%)	63.9
ion exchange capacity (mmol/g)	1.77 ± 0.08
density (g cm^{-3})	1.24 ± 0.01

[a] All measurements were made at room temperatures. See ref 10 for details.

In an effort to use the high conductivity of Nafion and still exploit the potential advantages of high-pH operation, we report here a hybrid fuel cell design that comprises at least one electrode operating at high pH. This is the first report of a hybrid fuel cell comprised of an AEM and PEM. Our attention is initially directed toward the electrochemical behavior at the AEM/PEM junction. The operating behavior of the AEM/PEM junction in a hybrid fuel cell is investigated.

Experimental Section

A Nafion solution (5% suspension by mass) was used as the ionomer in the fabrication of a low-pH electrode (PEM electrode). The high-pH electrode (AEM electrode) was made using an anion exchange ionomer (AEI), poly(arylene ether sulfone) functionalized with quaternary ammonium groups synthesized for this study, as described previously.[10] The ion exchange capacity (IEC) of the AEM was determined by a back-titration method.[11] The density of the AEM was calculated by the method that was used in the literature for the determination of the Nafion density.[12] The physical properties of the AEM are summarized in Table 1. The AEI was stored as a solution of 5% by mass in dimethylformamide (DMF). The Nafion membranes were pretreated with 3% H_2O_2 and 1 M H_2SO_4 solutions.

The catalyst ink for the low-pH electrode was prepared by mixing a Nafion solution, platinum supported on carbon (20% Pt), isopropyl alcohol (IPA), and water. The catalyst ink for the anionic, high-pH electrode was prepared by mixing the Pt/C catalyst and the AEI with a mixture of water and DMF (2:3 by mass). The catalyst inks were sonicated for 15 min and then

10.1021/jp903252u CCC: $40.75
Published on Web 06/04/2009

cast onto hydrophobic Toray carbon paper (TGPH-090). The resulting electrodes had a surface area of 2 cm^2 and catalyst loading of 0.5 mg/cm^2.

Two types of hybrid membrane electrode assembly (MEAs) were prepared. In the first type of hybrid MEA (HMEA-I), the AEM and PEM half-cells were prepared individually and then pressed together. For the AEM half-cell, the AEM electrode (Pt/C and ionomer on carbon paper) was pressed onto the AEM, ~150 μm thick, at a 2 MPa gauge pressure and room temperature for 3 min. Then the half-cell was soaked in 0.1 M NaOH to exchange the Cl^- ions in the ionomer for OH^-. For the PEM half-cell, 100 μL of a Nafion (5% suspension)/IPA mixture (1:2 by volume) was sprayed onto the carbon paper (TGPH-090). The PEM electrode (Pt/C, ionomer on carbon paper) was pressed onto Nafion 212 at a 2 MPa gauge pressure and 135 °C for 3 min. A 500 μL volume of the Nafion suspension (5% suspension)/IPA mixture (1:2 by volume) was sprayed onto the surface of the AEM before the two half-cells were pressed together. The two half-cells were then pressed together at room temperature and 2 MPa for 5 min. The AEM/PEM junction constitutes a bipolar membrane.

For the second type of hybrid MEA (HMEA-II), the AEM was not used in the half-cell and the anionic electrode was pressed directly onto the Nafion membrane. In this case, the AEM/PEM junction was formed close to the AEM electrode. A 50 μL volume of AEI in DMF (1% mass) was sprayed directly onto the surface of the AEM electrode. After being dried at room temperature, the AEM electrode was immersed in aqueous 0.1 M KOH to exchange OH^- for Cl^-. A 100 μL volume of the Nafion (5% suspension)/IPA mixture (1:2 by volume) was sprayed onto both the AEM and PEM electrodes before assembly of the electrodes onto the membrane. The MEA was assembled in two steps. In the first step, the PEM electrode was pressed onto Nafion 212 at a 2 MPa gauge pressure and 135 °C for 3 min. In the second step, the AEM electrode was pressed onto the PEM half-cell assembly at 2 MPa and ambient temperature for 3 min. Conventional PEM-based MEAs (PEM-MEAs) were prepared by the following protocol: A 100 μL volume of the Nafion (5% suspension)/IPA mixture (1:2 by volume) was first sprayed onto the PEM electrode. The PEM electrode was then pressed onto Nafion 212 at a 2 MPa gauge pressure and 135 °C for 3 min.

All MEAs were preconditioned by operating them in a fuel cell at steady state at a 600 mV discharge voltage for 24 h before $I-V$ polarization experiments were performed. Electrochemical measurements were performed using a PAR 2273 potentiostat/galvanostat. Fuel cell tests were conducted at ambient pressure. Electrochemical impedance spectra were measured, following polarization curves, in the constant-voltage mode using frequencies from 10 mHz to 10 kHz. The amplitude of the ac voltage was 10 mV.

Theory of the PEM/AEM Junction

The interface between the AEM and PEM is a critical part of the hybrid fuel cell. The electrochemical behavior of hybrid AEM/PEM junctions has been studied in electrodialysis applications for an electrochemical salt splitting into its corresponding acid and base.[13−15] The fixed charges in the AEM and PEM result in an interfacial phenomenon at the junction of two membranes. The electrochemical behavior of this junction is analogous to a semiconductor p−n junction where the mobile positive carriers in the PEM are hydrogen ions and the mobile negative carriers in the AEM are hydroxide ions.[16]

At the interface of an ideal PEM and AEM, mobile protons in the PEM and mobile hydroxide in the AEM can combine to form water. The immobile, anionic sulfonate groups remaining in the PEM create an electric field which electrostatically opposes the diffusion of additional protons from the PEM to the PEM/AEM junction, as shown in Figure 1. Likewise, the mobile hydroxide within the AEM will continue to diffuse to the PEM/AEM junction until the fixed quaternary ammonium groups within the AEM generate a field opposing the diffusion of additional hydroxide to the interface. At equilibrium, the net flux of protons in the PEM to the interface is zero because the flux to the interface due to diffusion, J_{H^+}(diffusion), is counterbalanced by the flux away from the interface due to migration, J_{H^+}(migration), eq 1. The same is true for hydroxide in the AEM, eq 2.

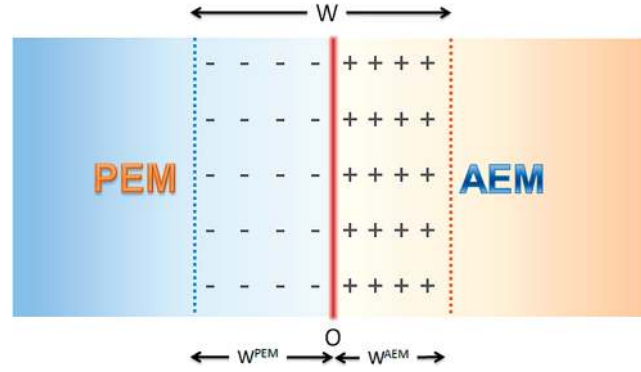

Figure 1. An illustration of the depletion region created at the junction of the AEM and PEM in contact.

$$J_{H^+}(\text{diffusion}) + J_{H^+}(\text{migration}) = 0 \quad (1)$$

$$J_{OH^-}(\text{diffusion}) + J_{OH^-}(\text{migration}) = 0 \quad (2)$$

Stated another way, protons in the PEM will continue to react with hydroxide in the AEM until the electrochemical potentials in the two phases become equal. That is, the difference in activity of the protons is counterbalanced by the potential difference in the two phases. The neutralization of the protons and hydroxide at the interface of the AEM and PEM leaves that region at a relatively neutral pH. An electric field, E, is generated by the fixed charges on each side of the interface, resulting in a potential difference between the two materials as illustrated in Figure 2. The gradient in the potential, $\phi_{(x)}$, is opposite to the field, $E_{(x)}$, as given by

$$E_{(x)} = -d\phi_{(x)}/dx \quad (3)$$

A quantitative relationship for the electric field and the activity of mobile ions can be obtained by expanding eq 1:

$$J_{H^+}(\text{net}) = 0 = q[\mu_{H^+} a_{H^+} E_{(x)} - D_{H^+}(da_{H^+}/dx)] \quad (4)$$

where q is the elementary charge, μ_{H^+} is the proton mobility, a_{H^+} is the activity of the protons, and D_{H^+} is the proton diffusivity. Equation 4 is expressed in one dimension, x, for simplicity. Equation 4 can be rearranged along with eq 3 and the Einstein relationship $\mu_{H^+}/D_{H^+} = q/kT$, where k is the Boltzmann constant and T is the temperature, yielding

$$-(q/kT)(d\phi_{(x)}/dx) = (1/a_{H^+})(da_{H^+}/dx) \quad (5)$$

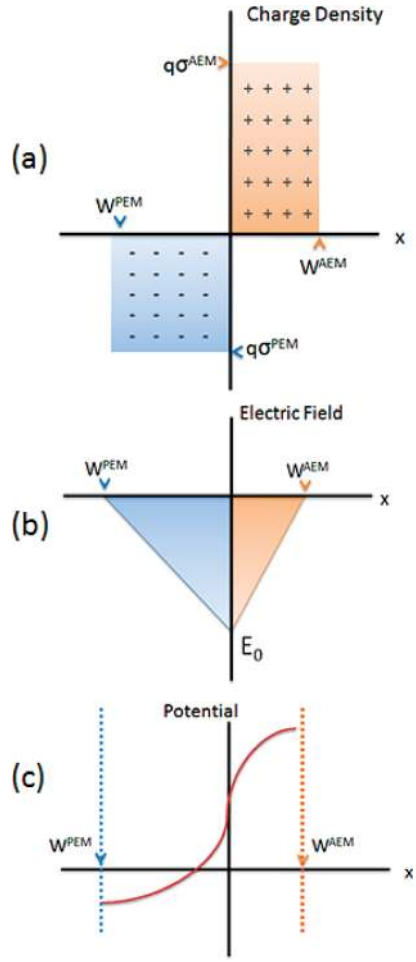

Figure 2. An illustration of the (a) space charge, (b) electric field, and (c) potential distribution within the transition region of the AEM/PEM junction.

where $\phi_{(x)}$ is the potential within the membrane as a function of the distance x going from the PEM to the AEM. Integration of eq 5 from the bulk of the PEM, ϕ^{PEM}, to the bulk of the AEM, ϕ^{AEM}, and the proton activity from the bulk of the PEM, $a_{H^+}^{PEM}$, to the bulk of the AEM, $a_{H^+}^{AEM}$, yields eq 6 or 7

$$E_j = \phi^{AEM} - \phi^{PEM} = (kT/q)\ln(a_{H^+}^{PEM}/a_{H^+}^{AEM}) \quad (6)$$

$$E_j = \phi^{AEM} - \phi^{PEM} = \frac{RT}{F}\ln(a_{H^+}^{PEM}/a_{H^+}^{AEM}) \quad (7)$$

(on a molar basis), where E_j is the contact potential between the AEM, ϕ^{AEM}, and PEM, ϕ^{PEM} and R is the ideal gas constant. It is assumed that hydroxide and protons are in equilibrium everywhere and $K_w = a_{H^+}a_{OH^-}$, which yields

$$E_j = \phi^{AEM} - \phi^{PEM} = \frac{RT}{F}\ln(a_{H^+}^{PEM}a_{OH^-}^{AEM}) - \frac{RT}{F}\ln(K_w) \quad (8)$$

If the activity of the protons in the PEM and hydroxide within the AEM were each at unit activity, then the contact or interface potential would be 0.83 V. The built-in or contact potential, E_j, cannot be directly measured by placing reference electrodes on each side of the junction because that would only create two more potentials which would exactly cancel E_j.

The absence of mobile ions at the junction zone between the ion exchange polymer electrolytes establishes a depleted electric double layer. The width of the depletion region, W, can be broken into two components:

$$W = W^{PEM} + W^{AEM} \quad (9)$$

where W^{PEM} is the width of the depletion region within the PEM and W^{AEM} is the width of the depletion region within the AEM (see Figure 1). Gauss's law defines a relationship between the electric field at any point, $E_{(x)}$, to the charge:

$$dE_{(x)}/dx = (q/\varepsilon)[N_A(a_{H^+}^{PEM} - a_{OH^-}^{AEM}) + N_+ - N_-] \quad (10)$$

where ε is the permittivity of the medium, N_A is Avogadro's number, and N_+ and N_- are the densities of fixed charges (number of ionic sites/cm^3) in the AEM and PEM, respectively. If we assume that the activity of the protons and hydroxide within the depletion region W are zero, then within the PEM $dE_{(x)}/dx = -(q/\varepsilon)N_-$ and within the AEM $dE_{(x)}/dx = (q/\varepsilon)N_+$. Integration yields an expression for the maximum electric field, E_0 (see Figure 2b):

$$E_0 = -(q/\varepsilon)N_-W^{PEM} = -(q/\varepsilon)N_+W^{AEM} \quad (11)$$

The field on each side of the membrane is proportional to the density of fixed charge. The potential difference across the junction, E_j, is simply the negative integral of the field, eq 11, with respect to the distance, x:

$$E_j = (q/2\varepsilon)N_+W^{AEM}W \quad (12)$$

An expression for the width of the full depletion region can be obtained from eq 12 by recognizing that the magnitude of the negative charge within the PEM is equal to the positive charge in the AEM at equilibrium, assuming complete neutralization of the protons and hydroxides within W:

$$N_-W^{PEM} = N_+W^{AEM} \quad (13)$$

Substitution of eq 13 into eq 12 yields an expression for the width of the depletion region as a function of the potential difference or density of fixed charge by use of eq 6:

$$W = \left[\frac{2\varepsilon E_j}{q}(1/N_+ + 1/N_-)\right]^{1/2} = \left[\frac{2\varepsilon kT}{q^2}(1/N_+ + 1/N_-)\ln(N_+N_-/K_w)\right]^{1/2} \quad (14)$$

The density of fixed charges, $N_\pm$, can be expressed by the IEC of polymer electrolytes by $N_\pm = N_A(IEC_\pm)\rho_m$, where N_A is Avogadro's number and ρ_m is the density of the polymer electrolyte. The IEC and ρ_m for Nafion 1100 are 0.9 mmol/g and 1.65 g/cm^3, respectively, from the literature.[12] The IEC of the AEM is 1.77 mmol/g and ρ_m is 1.24 g/cm^3, as determined here. These values correspond to a charge density of 1.32×10^{21} cm^{-3} for the AEM and 8.94×10^{20} cm^{-3} for the PEM. Considering the high water uptake of polymers at the AEM/

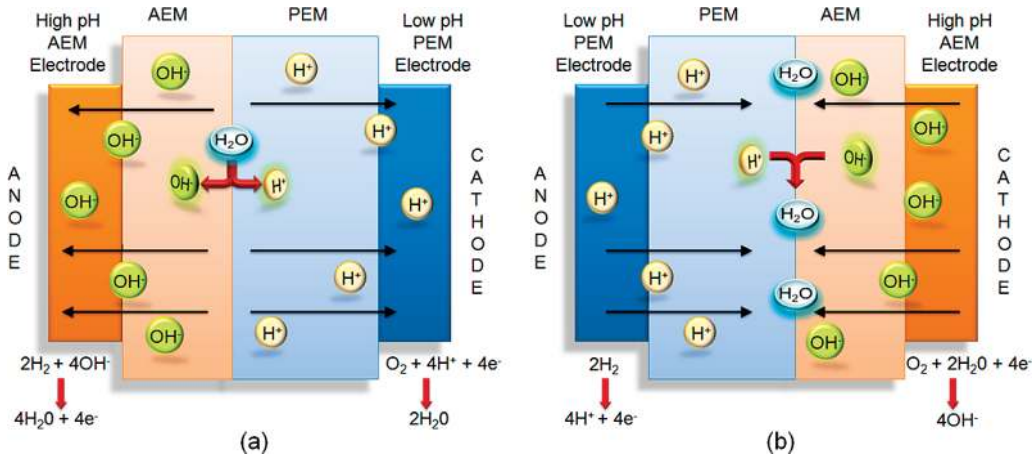

Figure 3. Operation mechanism of hybrid fuel cells comprising (a) a high-pH AEM anode/low-pH PEM cathode and (b) a low-pH PEM anode/high-pH AEM cathode.

PEM interface, the relative permittivity of the hydrated polymer junction can be estimated to be $\varepsilon = 35$ (or higher). If the activity of mobile ions in both phases is 1, the depletion layer is calculated to be 2.5 nm thick from eq 14. The depletion region on each side of the interface can also be determined:

$$W^{\mathrm{PEM}} = WN_{+}/(N_{+} + N_{-}) \quad (15)$$

$$W^{\mathrm{AEM}} = WN_{-}/(N_{+} + N_{-}) \quad (16)$$

This leads to a depletion region of 1.0 and 1.5 nm in the AEM and PEM, respectively. These values reveal that there is a large voltage gradient over a short distance at the membrane junction, contributing to the external voltage. It is important to emphasize that this model considered above is oversimplified by the assumption of an abrupt junction between two polymeric materials. In fact, there are the smooth variation of the membrane fixed charge concentration and the existence of a neutral region over the junction. Therefore, the actual depletion region is expected to be larger than the one presented above. In addition, the membranes modeled here were assumed ideal (i.e., only anions permeate through the AEM and only cations through the PEM), and a sharp, planar interface was assumed.

Results and Discussion

To investigate the electrochemical behavior of the AEM/PEM junction in an operating fuel cell, an HMEA-I cell was constructed. In this case, electrodes were fabricated onto the AEM and PEM prior to assembly together, as described in the Experimental Section. The AEM and PEM electrode assemblies were pressed together using Nafion ionomer solution to form the bipolar membrane, as shown in Figure 3. The total thickness of the bipolar membrane was 174 μm.

HMEA-I was initially tested with the AEM electrode operating as the anode and the PEM electrode as the cathode. Hydrogen gas at 50 °C and 100% relative humidity (measured at 50 °C) was used at the anode and oxygen gas at 50 °C and 100% relative humidity was used at the cathode, as shown in Figure 3a. The $I-V$ polarization curves are shown in Figure 4 (solid line). The open circuit voltage was 860 mV, and the maximum power density was 0.03 mW/cm^2. In this configuration, hydrogen is oxidized at the anode under alkaline conditions, forming water. The standard potential is more negative than for hydrogen under acidic conditions, eq 17.

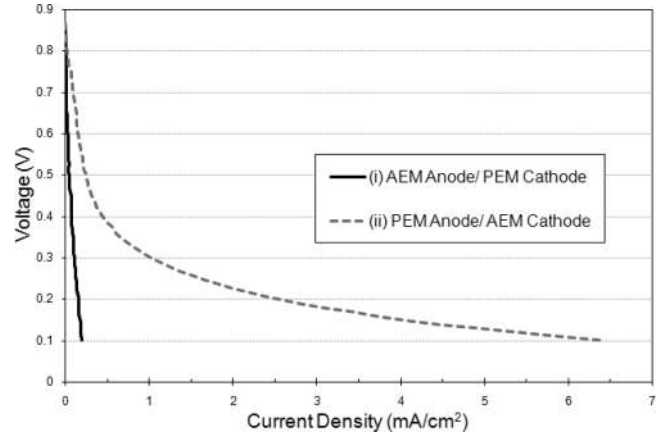

Figure 4. Polarization curves for a hybrid fuel cell (HMEA-I) comprising (i) a high-pH anode and (ii) a high-pH cathode with the bipolar membrane at 50 °C and atmospheric pressure. Gas feeds are humidified H_2 and O_2 with flow rates of 12 and 6 sccm, respectively.

Oxygen reduction takes place at the cathode at low pH, creating protons, resulting in the formation of water, eq 18.

$$\text{anode: } H_2 + 2OH^- \rightarrow 2H_2O + 2e^- \qquad E_A^0 = -0.83 \text{ V (SHE)} \quad (17)$$

$$\text{cathode: } {}^1/_2O_2 + 2H^+ + 2e^- \rightarrow H_2O \qquad E_C^0 = 1.23 \text{ V (SHE)} \quad (18)$$

In this configuration, OH^- migrates within the AEM toward the anode and H^+ within the PEM migrates toward the cathode, as shown in Figure 3a. As a result of the ion migration, the AEM/PEM junction is depleted of OH^- and H^+, forming a depletion layer at the junction. This depletion region leads to a junction potential, E_j, as summarized in the previous section. Water dissociation occurs at the interface, eq 19,[17,18] and the overall reaction is given by eq 20.

$$\text{interface: } 2H_2O \rightarrow 2OH^- + 2H^+ \quad (19)$$

$$\text{overall: } H_2 + {}^1/_2O_2 \rightarrow H_2O \quad (20)$$

However, for this configuration, the junction potential, E_j, constitutes an additional perturbation to the Nernst voltage:

$$E_{cell} = E_{Nernst} + E_j = E_C - E_A + E_j \quad (21)$$

$$E_{cell} = E_C^0 - E_A^0 + \frac{RT}{2F}\ln\left[\frac{P_{O_2}{}^{1/2}P_{H_2}}{P_{H_2O}}\right] + \frac{RT}{F}\ln[a_{OH^-}^{AEM}a_{H^+}^{PEM}] + E_j \quad (22)$$

where E_C is the cathode potential, E_A is the anode potential, and $E_j = \phi^{PEM} - \phi^{AEM} = (RT/F)\ln(K_w/a_{OH^-}^{AEM}a_{H^+}^{PEM})$ (from eq 8). It is noteworthy that the activity terms in the Nernst potential and the junction potential cancel each other. This leads to a formal cell potential equal to 1.23 V, eq 22, with a correction for the partial pressure of the gases, regardless of the pH of the AEM and PEM, eq 23.

$$E_{cell} = 1.23 + \frac{RT}{2F}\ln\left[\frac{P_{O_2}{}^{1/2}P_{H_2}}{P_{H_2O}}\right] \quad (23)$$

The HMEA-I configuration was reversed from the previous experiments with respect to the hydrogen and oxygen gases, as shown in Figure 3b. In this second configuration, hydrogen is consumed at the PEM anode at low pH and oxygen is consumed at the high-pH AEM cathode. Protons migrate from the anode to the PEM/AEM junction, and hydroxide migrates from the cathode to the PEM/AEM junction. Recombination of the proton and hydroxide at the junction forms water, Figure 3b. The fuel cell performance is shown in Figure 4 (dashed lines) for the H_2/O_2 cell at 50 °C. The open circuit voltage was 867 mV, and the maximum power density was 0.64 mW/cm^2. The current and power were substantially larger than in the first configuration (solid line, Figure 4) because formation of water at the PEM/AEM junction is more favorable than the water splitting in the first case, which quickly leads to dry-out of the membrane. The half-cell and overall reactions are given in the following equations:

$$\text{anode: } H_2 \rightarrow 2H^+ + 2e^- \quad E_A^0 = 0.00 \text{ V (SHE)} \quad (24)$$

$$\text{cathode: } {}^1/_2O_2 + H_2O + 2e^- \rightarrow 2OH^- \quad E_C^0 = 0.40 \text{ V (SHE)} \quad (25)$$

$$\text{interface: } 2OH^- + 2H^+ \rightarrow 2H_2O \quad (26)$$

$$\text{overall: } H_2 + {}^1/_2O_2 \rightarrow H_2O \quad E_{cell} = 1.23 \text{ V} \quad (27)$$

Although oxygen reduction in a high-pH environment occurs at lower potentials (0.4 V) than in the first set of experiments (low-pH counterpart, 1.23 V), the voltage loss at the cathode is compensated by the junction potential, $E_j = (RT/F)\ln(a_{OH^-}^{AEM}a_{H^+}^{PEM})$, which constitutes a positive bias to the cell voltage. Not surprising, the thermodynamic cell potential for the two sets of experiments is the same since the overall hydrogen/oxygen reaction is the same in both cases.

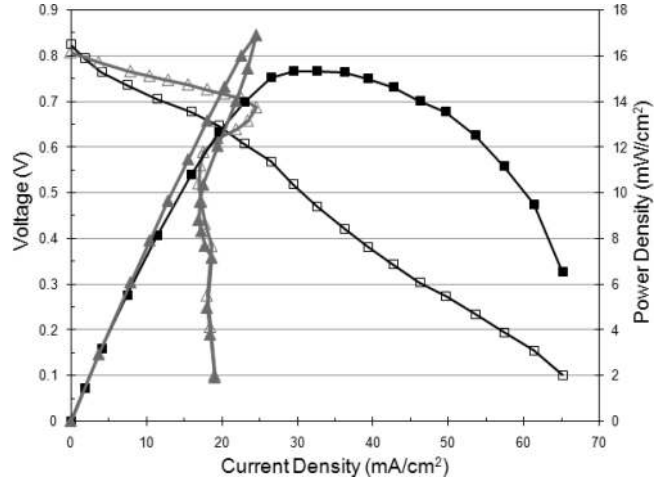

Figure 5. Polarization curves for a hybrid fuel cell (HMEA-II) comprising (△) a high-pH anode and (□) a high-pH cathode with a Nafion core membrane at 50 °C. Gas feeds are humidified H_2 and O_2 with flow rates of 12 and 6 sccm, respectively. Solid symbols correspond to the power density.

Although these two fuel cell configurations are useful in revealing the viability of hybrid MEA designs, the performances were low compared to those of hydrogen/oxygen PEM cells. The poor performance is likely due to nonoptimized fabrication methods for the bipolar membrane electrode assemblies and the large membrane thickness, causing high resistance.

A second hybrid MEA (HMEA-II) construction was undertaken. In HMEA-II, the AEM membrane was eliminated by forming the high-pH anionic conducting electrode directly on the Nafion PEM. In this way, the ionic resistance of the AEM material is avoided and the PEM/AEM junction occurs close to the AEM electrode. It is important to note that a thin layer of AEM ionomer was sprayed (solvent cast) on the AEM electrode surface to eliminate a possible contact between the Nafion membrane and the Pt/C catalyst in the AEM electrode assembly. The HMEA-II membrane assembly was initially tested with the AEM electrode (high pH) operating as the anode and the PEM electrode (low pH) as the cathode in a H_2/O_2 cell at 50 °C. The polarization curve is shown in Figure 5. The open circuit voltage was 801 mV, and the maximum power density was 16.9 mW/cm^2. Interestingly, the cell could not be operated at lower discharge voltages (higher current densities). This limitation is likely due to an inadequate flux of water to the AEM/PEM interface where water dissociates into hydrogen ions (which migrate to the cathode) and hydroxide (which migrates to the anode). That is, the depletion region which is created at the AEM/PEM junction due to deficiency of protons in PEM and hydroxides in AEM results in an electric field which drives water dissociation at the AEM/PEM interface, eq 19. The flow of current in the fuel cell relies on the continuous generation of protons and hydroxide from water dissociation at the AEM/PEM interface. Thus, the steady-state operation of the cell is limited by the flux of water to the AEM/PEM interface.

As with the HMEA-I cell, the HMEA-II cell assembly was operated in the reverse configuration where the AEM electrode was operated as the cathode and the PEM electrode was operated as the anode. The fuel cell performance is shown in Figure 5 for a H_2/O_2 cell at 50 °C. The open circuit voltage was 809 mV, and the maximum power density was 15.3 mW/cm^2. The

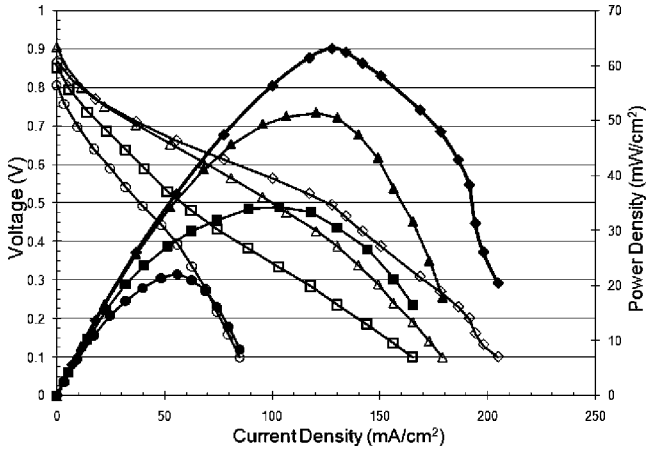

Figure 6. Polarization curves for a hybrid fuel cell (HMEA-II) comprising a high-pH cathode with a Nafion core membrane at 50 °C and a relative humidity of (△) 0%, (◇) 37%, (□) 80%, and (○) 100%. Gas feeds are humidified H_2 and O_2 with flow rates of 12 and 6 sccm, respectively. Solid symbols correspond to the power density.

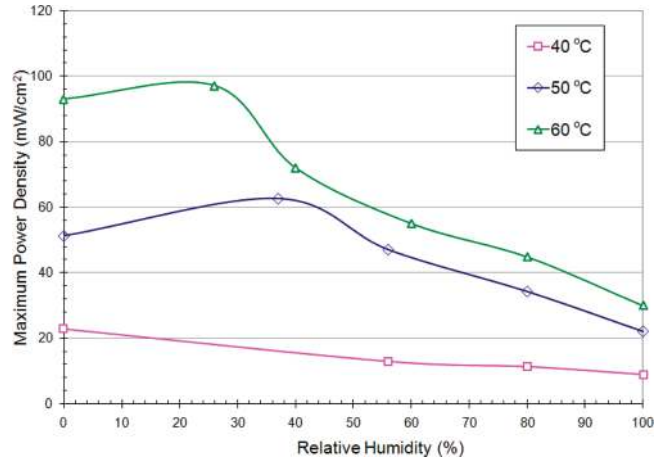

Figure 7. Peak power densities of a hybrid cell (HMEA-II) comprising the AEM cathode and PEM anode with a Nafion membrane for different relative humidities at (□) 40, (◇) 50, and (△) 60 °C.

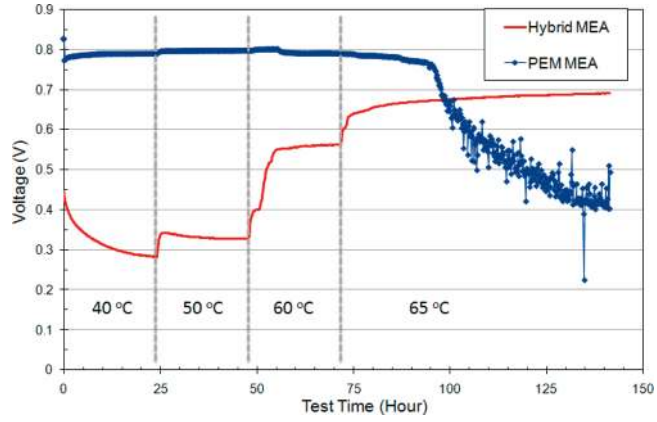

Figure 8. Cell voltages of HMEA-II and PEM/MEA as a function of time for a constant discharge load of 25 mA/cm^2 at different temperatures without external humidification. The flow rates are 0.8 sccm for H_2 and 0.6 sccm for O_2, corresponding to stoichiometries of 2 and 3, respectively.

power density was similar to that of the first configuration (AEM anode); however, the cell could be discharged at lower voltages.

There are two interesting changes that occur when HMEA-II is operated with the low-pH PEM electrode as the hydrogen anode and the high-pH AEM electrode as the oxygen cathode. First, it is known from alkaline fuel cell technology that oxygen reduction at high pH (producing OH^-) can occur on non-platinum electrodes since protonation of the intermediates, and subsequent catalytic decomposition, does not occur. Second, water is produced at the interface between the PEM and AEM, which creates a self-hydrating effect within the membrane. Figure 6 shows $I-V$ curves with 0%, 37%, 80%, and 100% relative humidity in the hydrogen and oxygen gas streams, both at 50 °C. Each $I-V$ curve was collected after constant-voltage operation at 600 mV for 24 h. There is a gradual decrease in the performance as the relative humidity increases. The maximum power density obtained was 63 mW/cm^2 at 37% relative humidity, whereas the power was 22 mW/cm^2 at 100% relative humidity. Dry operation (zero relative humidity in both gas streams) produced a power density of 52 mW/cm^2, which is higher than that of the 100% humidified condition. The self-hydration effect of the PEM/AEM configuration is shown in Figure 7 where the peak power densities are reported for each $I-V$ curve collected as a function of temperatures and relative humidity. At all temperatures, the cell performance increases as the relative humidity decreases. The performance at zero humidity is higher than that at the highly humidified conditions. Operation of the traditional Nafion-based PEM cell at 0% humidity would cause dry-out of the membrane. It is well established that the PEM cell performance decays when the relative humidity decreases because the ionic conductivity of the Nafion membrane electrolyte is related to the level of hydration.[19] Although there are reports showing self-hydrated fuel cells, the performance at zero humidity shows a gradual decay in the current when discharged under constant load.[20−22]

Figure 8 shows a side-by-side comparison of the cell performance of the hybrid MEA (HMEA-II) and a Nafion-based PEM fuel cell operated with dry H_2/O_2 feed at various temperatures. The cell temperature was raised from 40 to 65 °C in four steps. The fuel cells were discharged at 25 mA/cm^2, and the voltage was recorded. For the Nafion PEM cell, the potential remained at 800 mV at 40−50 °C. At these moderate temperatures, the cell can retain adequate hydration from back-diffusion of water produced at the cathode. When the temperature was increased to 60 °C, the voltage gradually decayed due to the dehydration of the Nafion MEA. The decay in discharge voltage is much steeper at 65 °C with a 50% drop after three days of operation. In contrast, the hybrid PEM/AEM fuel cell shows a rapid drop in cell voltage at 40 °C. When the temperature was increased, the cell voltage also increased. After three days of discharge at 65 °C, the cell voltage increased to 700 mV. This increase in the performance at higher temperature is likely due to the self-hydration of the membrane during operation. The formation of water at the AEM/PEM interface provides a constant supply of water for membrane conductivity and reaction at the cathode.

To assist in understanding the performance characteristics within the hybrid cell, electrochemical impedance spectroscopy (EIS) was used to diagnose the change in performance with humidity and temperature. At the current densities used here, it is reasonable to assume that the anode overpotential was negligible compared to the cathode overpotential.[23] Figure 9 shows EIS spectra collected at 600 mV for various relative humidity values at 50 °C. For all conditions, the EIS spectrum is a semicircle loop. Typically, the difference between the x-intercept values at the high- and low-frequency ends of the semicircle corresponds to the charge transfer resistance. The high-frequency x-intercept corresponds to the MEA ionic

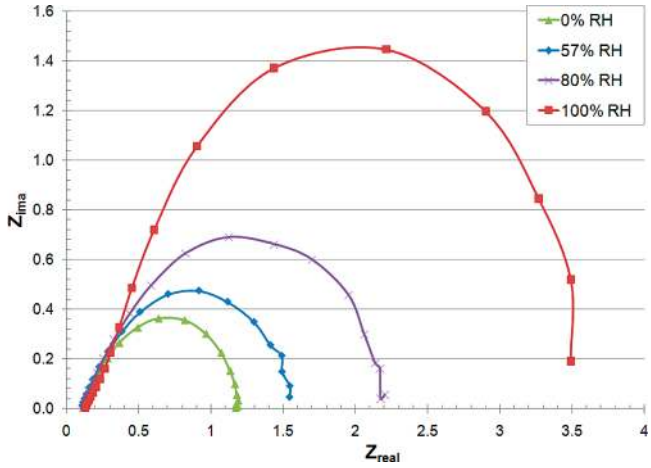

Figure 9. Impedance spectra of a hybrid cell (HMEA-II) collected at 600 mV for relative humidities of 0%, 57%, 80%, and 100%. The cell temperature is 50 °C. The flow rates are 12 sccm for H_2 and 6 sccm for O_2.

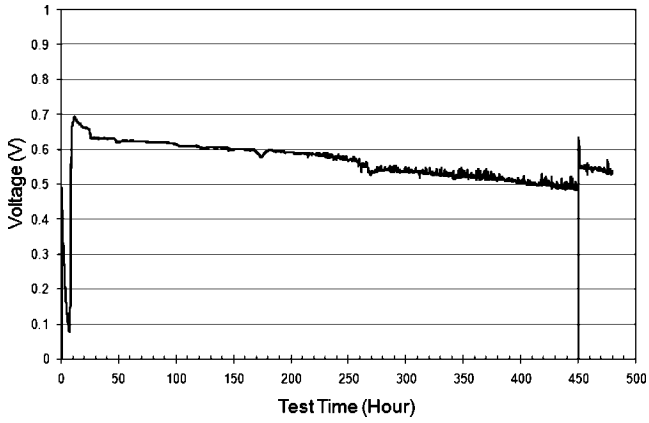

Figure 10. Cell voltage of HMEA-II as a function of time for a constant discharge load of 50 mA/cm^2 at 65 °C without external humidification. The flow rates are 5 sccm for H_2 and 4 sccm for O_2.

resistance.[24,25] These spectra show that the ionic resistance of the membrane remained nearly constant as a function of humidity; however, the charge transfer resistance increased with relative humidity. The effective charge transfer resistance is mainly determined by interfacial oxygen reduction kinetics, ionic conductivity, and diffusion limitations in the catalyst layer. Since the decrease in ionic conductivity of the PEM at high relative humidity is not expected, the diffusion limitation is the likely cause of the greater resistance at high humidity. Oxygen diffusion to the catalyst surfaces is probably inhibited by the excess water flood in the catalyst layers at high relative humidity.

The constant membrane resistance in Figure 9 is contrary to the typical response of Nafion-based PEM fuel cells. It is commonly observed in PEM cells that the high-frequency resistance increases as the relative humidity decreases due to dry-out of the membrane and the resulting decrease in ionic conductivity.[26] However, the hybrid PEM/AEM membrane did not dry-out due to the generation of water within the membrane as opposed to the generation of water at the cathode in a traditional PEM.

The discharge voltage of the AEM/PEM cell without humidification over a longer time period is shown in Figure 10. The performance slightly decays over time, decreasing from 698 to 496 mV after 450 h of operation. After the cell was stopped for 5 min at 450 h, the voltage increased to 550 mV. This observation suggests that the slight decrease in the performance is due to flooding in the electrode layer. The break time yields a dehydration of the MEA, resulting in higher voltage when the cell discharge was started again. The higher performance of the hybrid cell without external humidification is a result of water generation at the AEM/PEM junction. The electro-osmotic drag in the AEM is opposite that in a traditional PEM cell and mitigates some of the dry-out effect. However, at high relative humidity, the water content in the MEA, particularly in the cathode electrode, is too great, resulting in condensation and less oxygen at the reaction zone. This is seen in the impedance spectra where the charge transfer impedance increased at high-humidity conditions. Additionally, the drop in performance at 40 °C and 0% humidity (Figure 8) corresponds to the case where the self-hydration effect is excessive (at this lower temperature), causing cathode flooding and performance loss.

The overall performance of these hybrid cells is modest compared to that of conventional, humidified PEM fuel cells.[27] Clearly these membrane electrode assemblies have not been optimized. Work is under way to fabricate better electrodes using the ionomers synthesized here and optimized compositions.

Conclusions

The effect of the AEM/PEM junction on an operating fuel cell was evaluated. The AEM/PEM junction introduces an additional perturbation to the Nernst voltage, and its bias depends on the direction of the boundary. Regardless of the configuration of the hybrid cell, the junction potential at the AEM/PEM boundary balances the changes in the standard potential at the electrodes due to pH shift, resulting in a thermodynamic cell voltage of 1.23 V. The AEM anode/PEM cathode junction is shown to fail at high current density. This failure is attributed to the limited water transport to the boundary at which water dissociation maintains ionic conductivity. The operation at the AEM cathode/PEM anode junction was also shown to be a viable configuration. This configuration offers advantages compared to PEM-only fuel cells because a non-platinum cathode can be considered and self-humidification can allow operation under dry conditions. The hybrid cell operating at 0% relative humidity was demonstrated. Steady-state operation of the hybrid cell was demonstrated for long periods of time at 65 °C without external humidification, whereas the performance of the conventional PEM cell severely decreased over the same period of time. The overall performance of the hybrid cells is modest compared to that of conventional humidified PEM cells. The hybrid MEAs have not been optimized, and fabrication advances are under investigation to improve performance.

References and Notes

(1) Larminie, J.; Dicks, A. *Fuel Cell Systems Explained*; 2nd ed.; J. Wiley: Chichester, U.K., 2003.
(2) Nguyen, T. V.; White, R. E. *J. Electrochem. Soc.* **1993**, *140*, 2178–2186.
(3) Wee, J.-H.; Lee, K.-Y. *J. Power Sources* **2006**, *157*, 128–135.
(4) Yasuda, K.; Taniguchi, A.; Akita, T.; Ioroi, T.; Siroma, Z. *Phys. Chem. Chem. Phys.* **2006**, *8*, 746–752.
(5) Varcoe, J. R.; Slade, R. C. T. *Fuel Cells* **2005**, *5*, 187–200.
(6) McLean, G. F.; Niet, T.; Prince-Richard, S.; Djilali, N. *Int. J. Hydrogen Energy* **2002**, *27*, 507.
(7) Varcoe, J. R.; Slade, R. C. T.; Wright, G. L.; Chen, Y. *J. Phys. Chem. B* **2006**, *110*, 21041–21049.
(8) Spendelow, J. S.; Goodpaster, J. D.; Kenis, P. J. A.; Wieckowski, A. *J. Phys. Chem. B* **2006**, *110*, 9545–9555.
(9) Varcoe, J. R. *Phys. Chem. Chem. Phys.* **2007**, *9*, 1479–1486.
(10) Zhou, J.; Unlu, M.; Vega, J. A.; Kohl, P. A. *J. Power Sources* **2009**, *190*, 285–292.

(11) Danks, T. N.; Slade, R. C. T.; Varcoe, J. R. *J. Mater. Chem.* **2003**, *13*, 712–721.
(12) Oberbroeckling, K. J.; Dunwoody, D. C.; Minteer, S. D.; Leddy, J. *J. Anal. Chem.* **2002**, *74*, 4794–4799.
(13) Hurwitz, H. D.; Dibiani, R. *J. Membr. Sci.* **2004**, *228*, 17–43.
(14) Grossman, G. *J. Phys. Chem.* **1976**, *80*, 1616–1625.
(15) S Mafé, P. R. *Acta Polym.* **1997**, *48*, 234–250.
(16) Streetman, B. G. *Solid State Electronic Devices*; Prentice-Hall: Upper Saddle River, NJ, 1980.
(17) Hurwitz, H. D.; Dibiani, R. *Electrochim. Acta* **2001**, *47*, 759–773.
(18) Strathmann, H.; Rapp, H. J.; Bauer, B.; Bell, C. M. *Desalination* **1993**, *90*, 303–323.
(19) Zawodzinski, J. T. A.; Derouin, C.; Radzinski, S.; Sherman, R. J.; Smith, V. T.; Springer, T. E.; Gottesfeld, S. *J. Electrochem. Soc.* **1993**, *140*, 1041–1047.
(20) Buchi, F. N.; Srinivasan, S. *J. Electrochem. Soc.* **1997**, *144*, 2767–2772.
(21) Williams, M. V.; Kunz, H. R.; Fenton, J. M. *J. Power Sources* **2004**, *135*, 122–134.
(22) Tang, H. L.; Pan, M. *J. Phys. Chem. C* **2008**, *112*, 11556–11568.
(23) Ciureanu, M.; Wang, H. *J. Electrochem. Soc.* **1999**, *146*, 4031–4040.
(24) Raistrick, I. D. *Electrochim. Acta* **1990**, *35*, 1579–1586.
(25) Springer, T. E.; Zawodzinski, T. A.; Wilson, M. S.; Gottesfeld, S. *J. Electrochem. Soc.* **1996**, *143*, 587–599.
(26) Zhang, J.; Tang, Y.; Song, C.; Cheng, X.; Zhang, J.; Wang, H. *Electrochim. Acta* **2007**, *52*, 5095–5101.
(27) Qi, Z.; Kaufman, A. *J. Power Sources* **2003**, *113*, 37–43.

JP903252U